Constraining dark sector perturbations I: cosmic shear and CMB lensing

Richard A. Battye,[a] Adam Moss[b] and Jonathan A. Pearson[c]

[a]Jodrell Bank Centre for Astrophysics, School of Physics and Astronomy,
The University of Manchester, Manchester, M13 9PL, U.K.

[b]School of Physics & Astronomy, University of Nottingham,
Nottingham, NG7 2RD, U.K.

[c]Centre for Particle Theory, Department of Mathematical Sciences,
Durham University, South Road, Durham, DH1 3LE, U.K.

E-mail: richard.battye@manchester.ac.uk, adam.moss@nottingham.ac.uk,
jonathan.pearson@durham.ac.uk

Abstract. We present current and future constraints on equations of state for dark sector perturbations. The equations of state considered are those corresponding to a generalized scalar field model and time-diffeomorphism invariant $\mathcal{L}(g)$ theories that are equivalent to models of a relativistic elastic medium and also Lorentz violating massive gravity. We develop a theoretical understanding of the observable impact of these models. In order to constrain these models we use CMB temperature data from *Planck*, BAO measurements, CMB lensing data from *Planck* and the South Pole Telescope, and weak galaxy lensing data from CFHTLenS. We find non-trivial exclusions on the range of parameters, although the data remains compatible with $w = -1$. We gauge how future experiments will help to constrain the parameters. This is done via a likelihood analysis for CMB experiments such as CoRE and PRISM, and tomographic galaxy weak lensing surveys, focussing in on the potential discriminatory power of *Euclid* on mildly non-linear scales.

Contents

1 Introduction

There has been a recent explosion in the number of dark energy [1] and modified gravity [2] theories constructed in an attempt to describe the apparent observation of cosmic accelera-tion [3, 4]. It is now standard practice to include some "dark contribution" into the material content of the universe during the analysis of, e.g., observations of the temperature fluc-tuations in the Cosmic Microwave Background (CMB) [5] and gravitational lensing of the CMB [6, 7].

Observations of the CMB [6–10] and galaxy weak lensing [11, 12] are now mature enough to be able to use the current data to constrain some of the allowed properties of the dark sector (by which we mean dark energy and/or modified gravity, rather than dark matter). Recent dark energy constraints have focused on constraining the constant equation of state parameter w and "quintessence" sound speed c_s^2. Since these types of dark energy models do not cluster significantly, the constraints are rather weak [13–17]. There are a small number of constraints on a particular parameterization of modified gravity since the data release from *Planck* [18, 19]. Prospective CMB experiments such as the Polarized Radiation Imaging and Spectroscopy Mission (PRISM) [20] and Cosmic Origins Explorer (CoRE) [21], as well as future tomographic galaxy weak lensing experiments like the Dark Energy Survey (DES) [22], *Euclid* [23], and Large Synoptic Survey Telescope (LSST) [24], will considerably improve the constraining power. However, for any of these experiments to be used to their full potential, some framework for the evolution of possible perturbations in the dark sector is vital.

A useful framework for the dark sector at the level of the background already exists, and works very well: the dark contribution is modelled by the dark energy equation of state parameter $w = P/\rho$ (where P and ρ are the pressure and energy density of the dark fluid).

However, as soon as observational data are used which are sensitive to the clustering properties of the dark sector, some new framework needs to be employed. Such observations are those that are effected by the integrated Sachs-Wolfe effect and gravitational lensing. There is an abundance of parameterizations for perturbations of the dark sector in the literature [25–33], but a clear problem is emerging. A parameterization may well be constructed which covers the entire space of theories, but it will undoubtedly come with a huge number of free functions which experimental data will be unable to meaningfully constrain. Similarly, a very simple parameterization could be constructed which has a very small number of free parameters, but it may be too restrictive and will not probe wide enough ranges of theory space to yield theoretically meaningful results. And so: a balance which must be struck between theoretical generality and observational feasibility.

In this paper we will review and constrain the freedom in our *equations of state for perturbations* formalism. The parameterization contains all theories with a given field content and symmetries, and comes with a very small number of free parameters. This paper is complementary to [34], in which measurements of ISW and CMB lensing tomography are used to constrain the equations of state for perturbations.

The layout of this paper is as follows. In section 2 we explain and review the equations of state for perturbations formalism, as well as providing details of the models we consider. In section 3 we give some analytic evidence for the difference in the lensing potentials for classes of models with and without anisotropic stress: our fluids approach makes this particularly transparent. In section 4 we review the observational spectra which are used to obtain the data constraints presented in section 5. Section 6 describes the ability of future experiments at constraining the freedom in the models, and concluding remarks are saved for section 7.

2 Review of the formalism

2.1 Basic ideas

At its heart, the *equations of state for perturbations* formalism was designed to allow meaningful and model independent statements about the allowed properties of the dark sector to be extracted from observations. We will briefly review the formalism introduced and developed in [35–40].

The gravitational field equations for the class of theories we will study can be written as

$$G^\mu{}_\nu = 8\pi G \left[T^\mu{}_\nu + U^\mu{}_\nu\right], \tag{2.1}$$

where $T^\mu{}_\nu$ is the energy-momentum tensor of all known matter fields, and $U^\mu{}_\nu$ is the dark energy-momentum tensor which contains all contributions to the gravitational field equations due to the dark sector theory. This class of theories includes genuine dark energy models and also modified gravity models where $U^\mu{}_\nu$ includes, for example, higher derivatives of the metric. We will only study the minimally coupled dark sector here: this means that $T^\mu{}_\nu$ and $U^\mu{}_\nu$ are separately conserved. This restriction can, in principle, be relaxed.

For a background which is homogeneous and isotropic, $U^\mu{}_\nu$ can be specified in terms of two functions: the density, $\rho = \rho(t)$, and pressure, $P = P(t)$, of the dark sector fluid. The evolution of ρ is constrained by the conservation equation $\nabla_\mu U^\mu{}_\nu = 0$, giving $\dot\rho = -3\mathcal{H}(\rho + P)$ and hence the specification of an equation of state parameter, $w = P/\rho$, defines the evolution of the background.

The components of the perturbed dark energy-momentum tensor are parameterized as

$$\delta U^\mu{}_\nu = \delta\rho u^\mu u_\nu + 2(\rho + P)v^{(\mu}u_{\nu)} + \delta P\gamma^\mu{}_\nu + P\Pi^\mu{}_\nu, \qquad (2.2)$$

where $\delta\rho, v^\mu, \delta P$ and $\Pi^\mu{}_\nu$ are the perturbed fluid variables of the dark sector theory; we use round brackets to denote symmetrization of the enclosed indices, e.g., $A_{(\mu}B_{\nu)} = \frac{1}{2}(A_\mu B_\nu + A_\nu B_\mu)$. u^μ is a time-like vector and $\gamma^{\mu\nu} = u^\mu u^\nu + g^{\mu\nu}$ is the spatial metric, that is orthogonal to the time-like vector: $u^\mu\gamma_{\mu\nu} = 0$. The components of $\delta U^\mu{}_\nu$ are constrained by the perturbed fluid equations $\delta(\nabla_\mu U^\mu{}_\nu) = 0$, which, for scalar perturbations in the synchronous gauge, are

$$\dot\delta = (1+w)\left(k^2\theta^{\mathrm{S}} - \frac{1}{2}\dot h\right) - 3\mathcal{H}w\Gamma, \qquad (2.3\mathrm{a})$$

$$\dot\theta^{\mathrm{S}} = -\mathcal{H}(1-3w)\theta^{\mathrm{S}} - \frac{w}{1+w}\left(\delta + \Gamma - \frac{2}{3}\Pi^{\mathrm{S}}\right), \qquad (2.3\mathrm{b})$$

where the perturbed pressure δP has been packaged into the gauge invariant combination

$$w\Gamma \equiv \left(\frac{\delta P}{\delta\rho} - w\right)\delta. \qquad (2.4)$$

Here, $\delta, \theta^{\mathrm{S}}, \delta P$ and Π^{S} are the scalar parts of the perturbed dark sector fluid variables (note that we take $\dot w = 0$ for simplicity). In principle, knowledge of two of these functions specified the others through the equations of motion. In (2.3), Γ and Π^{S} are the gauge invariant entropy and anisotropic stress perturbations respectively and this property means that it is sensible to use these functions to specify the modified gravity/dark energy theory. The fluid equations (2.3) close when the entropy and anisotropic stress contributions are written as

$$w\Gamma = A_1\delta + A_2\theta^{\mathrm{S}} + A_3\dot h + \cdots, \qquad (2.5\mathrm{a})$$

$$w\Pi^{\mathrm{S}} = B_1\delta + B_2\theta^{\mathrm{S}} + B_3\eta + \cdots. \qquad (2.5\mathrm{b})$$

That is, when $w\Gamma$ and Π^{S} are specified as linear functions of variables which are already evolved (h and η are the metric perturbations in the synchronous gauge, as defined in [41]); note that the $\{A_i, B_i\}$ are chosen so that Γ and Π^{S} are gauge invariant. The entropy $w\Gamma$ and anisotropic stress $w\Pi^{\mathrm{S}}$ written in the form of (2.5) are the *equations of state for perturbations*.

The main idea behind our approach is to specify two ingredients: (i) the field content of the dark sector, and (ii) ask for a particular set of symmetries or principles to be respected and not to specify the actual Lagrangian. After these two ingredients are laid down, we are able to obtain *all the freedom* at the level of linearized perturbations, since these two ingredients are sufficient information for obtaining a precise form of the coefficients $\{A_i, B_i\}$ in the equations of state for perturbations (with prescribed scale dependence), and there will be nothing else left to specify to characterize the perturbations. In the next section we will provide the explicit examples we will be constraining in this paper.

Clearly, what we could do is to write down the largest field content and the smallest set of symmetries imaginable, but the problem is that this would create more free parameters than current (and near-future) cosmological data sets are able to constrain. This generalization is not of practical interest, at least for the foreseeable future.

2.2 Survey of models

Here we will describe what classes of models each of our equations of state for perturbations describes, and the number of associated free parameters. Our models have actions given by

$$S = \int d^4x \sqrt{-g} \left[\frac{R}{16\pi G} - 2\mathcal{L}(X) \right] + S_m[g_{\mu\nu}; \Psi_i].$$ (2.6)

As described above, each model is just a statement of the field content "X" in the dark sector Lagrangian $\mathcal{L}$ and a set of symmetries (typically, but not exclusively, taken to be reparameterization invariance). We do not need to specify the functional form of the dark sector Lagrangian.

2.2.1 Generalized scalar field models

For all models with field content

$$\mathcal{L} = \mathcal{L}(\phi, \partial_\mu \phi, \partial_\mu \partial_\nu \phi, g_{\mu\nu}, \partial_\alpha g_{\mu\nu}),$$ (2.7)

which are reparameterization invariant, have second order field equations, and are linear in $\partial_\alpha g_{\mu\nu}$, the equation of state for perturbations is [38]

$$w\Gamma = (\alpha - w) \left[\delta - 3\beta_1 \mathcal{H}(1+w)\theta^S - \frac{3\beta_2 \mathcal{H}(1+w)}{2k^2 - 6(\dot{\mathcal{H}} - \mathcal{H}^2)} \dot{h} + \frac{3(1 - \beta_2 - \beta_1)\mathcal{H}(1+w)}{6\ddot{\mathcal{H}} - 18\mathcal{H}\dot{\mathcal{H}} + 6\mathcal{H}^3 + 2k^2\mathcal{H}} \ddot{h} \right],$$ (2.8)

and $\Pi^S = 0$. We call this class of theories the generalized scalar field (GSF) theories. There are just three free dimensionless functions, $\mathcal{F} \equiv \{\alpha, \beta_1, \beta_2\}$. α and β_2 only depend on time, but in general β_1 will have scale dependence given by $\beta_1 = \beta_1^{(0)}(t) + \beta_1^{(2)}(t)k^2$ as explained in [38]. In models where $\beta_1^{(2)} \neq 0$ such theories will diverge as $k \to \infty$ and, hence, we set $\beta_1^{(2)} \equiv 0$, and we are left with three free dimensionless functions of time.

It is important to realize that *every* theory in this class is covered by these three functions. In particular, the kinetic gravity braiding [42, 43] theories are included, as are all cubic galileon theories [44].

As a subset of these theories, consider the dark sector Lagrangian with field content

$$\mathcal{L} = \mathcal{L}(\phi, \partial_\mu \phi, g_{\mu\nu}),$$ (2.9)

which are also reparameterization invariant. The gauge invariant equations of state for perturbations are [13, 45]

$$w\Gamma = (\alpha - w)\left[\delta - 3\mathcal{H}(1+w)\theta^S \right], \qquad \Pi^S = 0.$$ (2.10)

There is a single parameter, α, which can be interpreted as a sound speed for sub-horizon modes. It is clear that this simple scalar field model (2.10) is recovered from the general case (2.8) when $\beta_1 = 1, \beta_2 = 0$. The equation of state for perturbations (2.10) contains all minimally coupled k-essence theories whose Lagrangian is $\mathcal{L} = \mathcal{L}(\phi, \mathcal{X})$, where $\mathcal{X} \equiv -\frac{1}{2}(\partial\phi)^2$; the important point to realise is that by dialing the value of α, one dials through *all possible* $\mathcal{L} = \mathcal{L}(\phi, \mathcal{X})$ theories.

If a functional form of the Lagrangian is known, then $\alpha = (1 + 2\mathcal{X}\mathcal{L}_{,\mathcal{X}\mathcal{X}}/\mathcal{L}_{,\mathcal{X}})^{-1}$. When $\alpha = 1$, (2.10) describes perturbations of minimally coupled quintessence, and when $\alpha = w$ the adiabatic perturbations of shift-symmetric k-essence.

The theory whose Lagrangian is given by

$$\mathcal{L}(\phi, \mathcal{X}) = \left(-\mathcal{X} + \frac{\mathcal{X}^2}{M^4} \right) V(\phi),$$ (2.11)

where M is a mass scale and V an arbitrary function of ϕ, has α related to w via

$$\alpha = \frac{1 + w}{5 - 3w}.$$ (2.12)

2.2.2 Time diffeomorphism invariant $\mathcal{L}(g)$ theories

This class of models is rather distinct from the other classes of models we will discuss. These are constructed from a dark sector theory whose field content is

$$\mathcal{L} = \mathcal{L}(g_{\mu\nu}),$$ (2.13)

and is constrained to be invariant under time diffeomorphisms, but not space diffeomorphisms. This leaves a residual vector degree of freedom and a massive graviton. We call this class of theories the time diffeomorphism invariant (TDI) $\mathcal{L}(g)$ theories. These TDI $\mathcal{L}(g)$ theories have been studied in the literature, under the name of *elastic dark energy* [46–48]; the theory is equivalent to a particular brand of Lorentz violating massive gravities [37].

The equations of state for perturbations of the TDI $\mathcal{L}(g)$ models are

$$w\Gamma = 0, \qquad w\Pi^{\mathrm{S}} = \frac{3}{2}(w - c_{\mathrm{s}}^2)\big[\delta - 3(1 + w)\eta\big],$$ (2.14)

where η is the synchronous gauge metric perturbation. There is a single parameter, c_{s}^2, which is the sound speed of the medium. Notice that the medium is adiabatic (i.e., the entropy perturbation vanishes), but has an anisotropic stress. We should note that this theory represents one of the simplest possible ways to modify General Relativity.

2.3 Summary

Once the perturbed fluid equations (2.3) are furnished with one of the equations of state for perturbations, i.e., (2.8) or (2.14), the system of perturbation equations closes. In figure 1 we summarize the field contents, symmetries, and the associated number of free functions.

In the rest of the paper we observationally constrain allowed values of the free parameters: c_{s}^2 in the TDI $\mathcal{L}(g_{\mu\nu})$ models, and $\{\alpha, \beta_1, \beta_2\}$ in the GSF models. In this paper we restrict these parameters, and w, to be constant. We are simply being realistic about the constraining power of the available data.

This constraint of constancy calls into question what portion of the GSF theories are actually covered by taking $\{\alpha, \beta_1, \beta_2\}$ as constant. However, if we are able to observationally constrain the characteristic size of these parameters, particularly if one of them has to be small, then we have in-fact used data to learn something about the allowed properties of the dark sector theory. By measuring the constant values of these parameters we are measuring something which is characteristic to the evolution of perturbations of theories of a given class.

3 Evolution of the density contrast

We have cast our parameterization in terms of hydrodynamic quantities, and this can be used to obtain a simple, physically intuitive understanding of the role of the parameters in the

$$\mathcal{L} = \mathcal{L}\left(\phi, \partial_\mu \phi, \partial_\mu \partial_\nu \phi, g_{\mu\nu}, \partial_\alpha g_{\mu\nu}\right) \xrightarrow{\text{restrict}} \mathcal{L} = \mathcal{L}\left(\phi, \partial_\mu \phi, g_{\mu\nu}\right) \xrightarrow{\text{restrict}} \mathcal{L} = \mathcal{L}\left(g_{\mu\nu}\right)$$

$$\text{diff.inv} \Big\downarrow \qquad\qquad\qquad \text{diff.inv} \Big\downarrow \qquad\qquad \text{TDI} \Big\downarrow$$

$$\{\alpha, \beta_1, \beta_2\} \xrightarrow{\quad \beta_1 = 1, \beta_2 = 0 \quad} \{\alpha\} \qquad\qquad \{c_{\rm s}^2\}$$

figure 1. Schematic depiction of how the field content and symmetries of the models we study are related. The field content on the far left (2.7) is imposed with reparameterization invariance (and second order field equations, as well as being linear in $\partial_\alpha g_{\mu\nu}$ for simplicity) to yield the three parameters $\{\alpha, \beta_1, \beta_2\}$ in the equation of state for perturbations (2.8). Restricting the field content to (2.9) and then imposing reparameterization invariance leaves a single parameter, α, in the equation of state for perturbations (2.10). Further restriction of the field content to (2.13) and then imposing time diffeomorphism invariance leaves a single parameter, $c_{\rm s}^2$ in the equations of state for perturbations (2.14).

equations of state for perturbations, and why they take on certain values could potentially yield an observable effect. In this section we will have a brief look at the evolution equations of the density contrast of the dark energy fluid, paying special attention to the qualitative difference in the evolution equation and lensing potential for a fluid with non-zero entropy and anisotropic stress.

Combining the fluid equations (2.3) yields a second order evolution equation for the dark energy density contrast,

$$\begin{aligned}
&\ddot{\delta} + \mathcal{H}(1 - 3w)\dot{\delta} + k^2 w\delta \\
&= -\left[k^2 + 3\mathcal{H}^2(1 - 3w) + 3\dot{\mathcal{H}}\right] w\Gamma - 3\mathcal{H}w\dot{\Gamma} + \frac{2}{3}k^2 w\Pi - \frac{1}{2}(1 + w)\left[\ddot{h} + \mathcal{H}(1 - 3w)\dot{h}\right].
\end{aligned} \tag{3.1}$$

On a Minkowski background (obtained by setting $a = 1$), the evolution equation (3.1) becomes

$$\ddot{\delta} + k^2 w\delta = -k^2\left(w\Gamma - \frac{2}{3}w\Pi\right) - \frac{1}{2}(1 + w)\ddot{h}. \tag{3.2}$$

We are interested in models with $w < -1/3$, so that the fluid accelerates the universe, but without problematic gravitational instability which would be present for an adiabatic perfect fluid: if $w\Gamma = w\Pi = 0$, the density contrast only has exponential solutions when $w < 0$, indicating the undesirable gravitational instability. However, in the GSF (2.8) and TDI $\mathcal{L}(g)$ (2.14) models, (3.2) becomes

$$\ddot{\delta} + \alpha k^2 \delta = -\frac{1}{2}(1 + w)\ddot{h}, \tag{3.3a}$$

$$\ddot{\delta} + c_{\rm s}^2 k^2 \delta = -\frac{1}{2}(1 + w)\left[\ddot{h} + 6k^2(w - c_{\rm s}^2)\eta\right], \tag{3.3b}$$

respectively. Although both of these models are stable for $w < 0$, the physical origin is subtly different. In (3.3a) perturbations are supported against exponential growth by the sound speed α of a fluid with entropy (non-adiabatic pressure) perturbations, whilst in (3.3b) perturbations are supported due to the medium's anisotropic stress. It is clear that perturbations in both cases are subluminal and stable when $0 \leq \alpha \leq 1$ and $0 \leq c_{\rm s}^2 \leq 1$.

As we pointed out above, the physical origin of the protection against instability is different in the two cases: one was due to entropy, the other due to anisotropic stress. We can further elucidate this distinction by using the perturbed gravitational field equations to replace the metric fluctuations on the right-hand-sides of (3.3). In the synchronous gauge, with $a = 1$, the perturbed gravitational field equations are given by

$$-2k^2\eta = 8\pi G \sum_i \rho_i \delta_i, \tag{3.4a}$$

$$\dot{\eta} = -4\pi G \sum_i (\rho_i + P_i)\theta_i, \tag{3.4b}$$

$$\ddot{h} - 2k^2\eta = -24\pi G \sum_i \delta P_i, \tag{3.4c}$$

$$\ddot{h} + 6\ddot{\eta} - 2k^2\eta = -16\pi G \sum_i P_i \Pi_i, \tag{3.4d}$$

where the index "i" runs over all gravitating components: radiation, matter, and dark energy. After using (3.4) to replace all metric fluctuations in the combined perturbed fluid equations, one obtains the following second order evolution equation for the density contrast of component "i":

$$\ddot{\delta}_i + w_i k^2 \delta_i = -k^2 \left(w_i \Gamma_i - \frac{2}{3} w_i \Pi_i \right) + 4\pi G(1 + w_i) \sum_j \rho_j \left[3w_j \Gamma_j + (1 + 3w_j)\delta_j \right]. \tag{3.5}$$

Suppose that there are two components: "dark energy" and matter, $i \in \{m, de\}$. The equations of state for perturbations for both the GSF and TDI $\mathcal{L}(g)$ models yields the following sets of coupled evolution equations

- GSF

$$\ddot{\delta}_m - 4\pi G\rho_m \delta_m = 4\pi G(1 + 3\alpha)\rho_{de}\delta_{de}, \tag{3.6a}$$

$$\ddot{\delta}_{de} + \left[k^2\alpha - 4\pi G\rho_{de}(1 + w)(1 + 3\alpha) \right] \delta_{de} = 4\pi G\rho_m(1 + w)\delta_m. \tag{3.6b}$$

- TDI $\mathcal{L}(g)$

$$\ddot{\delta}_m - 4\pi G\rho_m \delta_m = 4\pi G(1 + 3w)\rho_{de}\delta_{de}, \tag{3.7a}$$

$$\ddot{\delta}_{de} + \left[c_s^2 k^2 - 4\pi G\rho_{de}(1 + w)\left(1 + 6w - 3c_s^2\right) \right] \delta_{de} = 4\pi G\rho_m(1 + w)\left[1 + 3(w - c_s^2)\right]\delta_m. \tag{3.7b}$$

Here we see that the evolution equations of the matter and dark energy density contrasts are qualitatively different in the two cases. To begin, notice that the source terms of the matter evolution equations (3.6a) and (3.7a) are different: the GSF case is multiplied by $(1 + 3\alpha)$, but the TDI $\mathcal{L}(g)$ case is multiplied by $(1 + 3w)$. Secondly, both the mass and source terms of the dark energy evolution equations (3.6b) and (3.7b) are qualitatively different.

Using the standard relations between the synchronous and conformal Newtonian gauges [41] we can obtain an expression for the lensing potential for this mixture of matter and dark energy

$$K^2(\phi + \psi) = -2 \left(\delta_m + R \left[\delta_{de} + w_{de}\Pi_{de} \right] \right), \tag{3.8}$$

where $R \equiv \rho_{\rm de}/\rho_{\rm m}$ and $K \equiv (4\pi G\rho_{\rm m})^{-1/2}k$. It is now clear that the anisotropic stress of dark energy has a non-trivial effect on the (observable) lensing potential. In order to elucidate the distinction in the lensing potential for models with and without anisotropic stress, we will compute the normal modes of the equations of motion (3.5) and express the lensing potential in terms of the growing and oscillating modes.

In the GSF and TDI $\mathcal{L}(g)$ cases the equations of motion can be written as $\mathbf{x}'' + \mathsf{A}\mathbf{x} = 0$, where $\mathbf{x} = \left(\begin{smallmatrix} \delta_{\rm m} \\ \delta_{\rm de} \end{smallmatrix}\right)$ and the primes denote derivative with respect to rescaled time, $T \equiv (4\pi G\rho_{\rm m})^{1/2}t$. The matrix A for each of the equations of motion (3.6) and (3.7) is given by

$$\mathsf{A}_{\rm GSF} = \begin{pmatrix} -1 & -R(1+3\alpha) \\ -\epsilon & K^2\alpha - R(1+3\alpha)\epsilon \end{pmatrix}, \tag{3.9}$$

$$\mathsf{A}_{\rm TDI} = \begin{pmatrix} -1 & -R(1+3w) \\ -(1+3Q)\,\epsilon & c_{\rm s}^2 K^2 - R(1+3[w+Q])\epsilon \end{pmatrix}, \tag{3.10}$$

respectively, where $\epsilon = 1+w$ and $Q = w - c_{\rm s}^2$. The signs of the eigenvalues of the matrix A determines what type of solutions the matter and dark energy density contrasts posess: if $\lambda > 0$, then solutions are oscillatory, and if $\lambda < 0$ they are exponential and correspond to growing modes. We will construct the modes $\eta \equiv \delta_{\rm m} + \mu\delta_{\rm de}$ that satisfy $\eta'' + \lambda\eta = 0$.

One can verify that when $\alpha = 0$ the GSF models have a zero eigenvalue for any value of w. For GSF models with $\alpha = 0$ we form the combinations which correspond respectively to the growing and zero eigenmodes,

$$\eta_{\rm grow}^{\rm (GSF)} = \delta_{\rm m} + R\delta_{\rm de}, \tag{3.11a}$$

$$\eta_{\rm zero}^{\rm (GSF)} = \delta_{\rm m} - \frac{\delta_{\rm de}}{\epsilon}. \tag{3.11b}$$

The existence of a zero mode is not shared by TDI models with $c_{\rm s}^2 = 0$, and as such it isn't possible to get such aesthetically pleasing forms of the modes in the TDI model for general w. However, expanding for small ϵ reveals that there are growing and oscillatory modes, which are given by

$$\eta_{\rm grow}^{\rm (TDI)} = \delta_{\rm m} - \left[2R - 3R(1+6R)\epsilon + \mathcal{O}(\epsilon)^2\right]\delta_{\rm de}, \tag{3.12a}$$

$$\eta_{\rm osc}^{\rm (TDI)} = \delta_{\rm m} + \left[\frac{1}{2\epsilon} + \frac{3}{4}(1+6R) + \frac{9}{8}\left(1 - 2R - 16R^2\right)\epsilon + \mathcal{O}(\epsilon)^2\right]\delta_{\rm de}. \tag{3.12b}$$

Substituting the GSF modes (3.11) into the lensing potential (3.8) reveals that

$$K^2(\phi + \psi) = -2\eta_{\rm grow}^{\rm (GSF)}, \tag{3.13}$$

and putting the TDI modes (3.12) into the lensing potential (3.8) yields

$$K^2(\phi + \psi) = \left[-2 + 3R\left(4 + 3K^{-2}\right)\epsilon + \mathcal{O}(\epsilon)^2\right]\eta_{\rm grow}^{\rm (TDI)} + \left[-12R\epsilon + \mathcal{O}(\epsilon)^2\right]\eta_{\rm osc}^{\rm (TDI)}. \tag{3.14}$$

There are some important properties and distinctions between these expressions for the lensing potential. We first remind that both are given at $a = 1$ and for $\alpha = c_{\rm s}^2 = 0$. The GSF lensing potential (3.13) is valid for any value of w, and only depends on one mode (the

growing mode) without any prefactors of the (rescaled) wavenumber K^2. The TDI lensing potential (3.14) includes both the growing and oscillating mode: the former also comes with a K^{-2}-dependence at $\mathcal{O}(\epsilon)$, and the latter only appears at $\mathcal{O}(\epsilon)$.

We now generalize to the case where $\alpha \neq 0$ and $c_{\mathrm{s}} \neq 0$. All expressions are sufficiently complicated that we exclusively expand to first order in ϵ. The eigenvalues of A are

$$\lambda_{\mathrm{grow}}^{(\mathrm{GSF})} = -\left[1 + R\frac{1+3\alpha}{1+K^2\alpha}\epsilon + \mathcal{O}(\epsilon)^2\right], \tag{3.15a}$$

$$\lambda_{\mathrm{osc}}^{(\mathrm{GSF})} = K^2\alpha\left[1 - R\frac{1+3\alpha}{1+K^2\alpha}\epsilon + \mathcal{O}(\epsilon)^2\right]; \tag{3.15b}$$

$$\lambda_{\mathrm{grow}}^{(\mathrm{TDI})} = -\left[1 + 2R\frac{2+3c_{\mathrm{s}}^2}{1+K^2c_{\mathrm{s}}^2}\epsilon + \mathcal{O}(\epsilon)^2\right], \tag{3.16a}$$

$$\lambda_{\mathrm{osc}}^{(\mathrm{TDI})} = K^2c_{\mathrm{s}}^2 + \frac{R}{1+K^2c_{\mathrm{s}}^2}\left[9\left(1+c_{\mathrm{s}}^2\right) + (5+3c_{\mathrm{s}}^2)K^2c_{\mathrm{s}}^2\right]\epsilon + \mathcal{O}(\epsilon)^2. \tag{3.16b}$$

The lensing potential in the GSF case is given by

$$
\begin{aligned}
&K^2(\phi+\psi) \\
&= \left[-2 + 2R\alpha\frac{3-K^2}{(1+K^2\alpha)^2}\epsilon + \mathcal{O}(\epsilon)^2\right]\eta_{\mathrm{grow}}^{(\mathrm{GSF})} + \left[-2R\alpha\frac{3-K^2}{(1+K^2\alpha)^2}\epsilon + \mathcal{O}(\epsilon)^2\right]\eta_{\mathrm{osc}}^{(\mathrm{GSF})},
\end{aligned}
\tag{3.17}
$$

and in the TDI case by

$$
\begin{aligned}
&K^2(\phi+\psi) \\
&= \Bigg[-2 + \frac{R}{(1+K^2c_{\mathrm{s}}^2)^2} \\
&\qquad \times \left(9\left(1+c_{\mathrm{s}}^2\right)K^{-2} + 6\left(2+9c_{\mathrm{s}}^2\right) + c_{\mathrm{s}}^2\left(4+15c_{\mathrm{s}}^2+9c_{\mathrm{s}}^3\right)K^2\right)\epsilon + \mathcal{O}(\epsilon)^2\Bigg]\eta_{\mathrm{grow}}^{(\mathrm{TDI})} \\
&\quad + \left[-2R\frac{\left(2+3c_{\mathrm{s}}^2\right)\left(3+K^2c_{\mathrm{s}}^2\right)}{(1+K^2c_{\mathrm{s}}^2)^2}\epsilon + \mathcal{O}(\epsilon)^2\right]\eta_{\mathrm{osc}}^{(\mathrm{TDI})}.
\end{aligned}
\tag{3.18}
$$

These are written in terms of the modes $\{\eta_{\mathrm{grow}}, \eta_{\mathrm{osc}}\}$ which are easily computed, but we omit for brevity.

The manipulations (with $a = 1$) we have presented highlights the qualitative difference in the evolution equations of the density contrasts in the two cases where the dark energy fluid has entropy and anisotropic stress. One of the important distinctions we draw out from this analysis is the manner in which each mode influences the lensing potential, and the different scale dependences of the coefficients of the modes involved. This distinction will be fully vindicated when we evolve the equations of motion in the next section.

4 Observational quantities

Let us, first, briefly review the observational probes we intend to use to constrain the equations of state for dark sector perturbations. We use a modified version of CAMB [49] to evolve the gravitational field equations with a dark sector fluid whose perturbations are parameterized via equations of state. This provides the gravitational potentials which can be used to compute all observational quantities we will discuss.

We stress that the modification to CAMB is minimal (of the order 10 lines of code): the equations of state involve quantities which are already evolved (or are trivially computable). This is in stark contrast to, e.g., the modifications to CAMB that are required for the slip and effective gravitational coupling parameterizations in MGCAMB [50].

We compute the usual CMB observables: the CMB temperature and polarization angular power spectra, as well as the CMB lensing power spectrum, $C_\ell^{\phi\phi}$. We also compute the galaxy lensing convergence power spectrum, $P_{ij}^\kappa(\ell)$, which in the absence of anisotropic stress can be written in terms of the matter power spectrum, $P(k, z)$. However, since our models include anisotropic stress, we use the more general form of the convergence power spectrum

$$P_{ij}^\kappa(\ell) \approx 2\pi^2 \ell \int \frac{\mathrm{d}\chi}{\chi} g_i(\chi) g_j(\chi) P_\Psi(\ell/\chi, \chi), \tag{4.1}$$

where we have made use of the Limber approximation in flat space, χ is the comoving distance, and P_Ψ is the power spectrum of the Weyl potential, defined in terms of the Newtonian potentials ϕ and ψ by $\Psi = (\psi + \phi)/2$. The lensing efficiency is given by

$$g_i(\chi) = \int_\chi^\infty \mathrm{d}\chi' n_i(\chi') \frac{\chi' - \chi}{\chi'}, \tag{4.2}$$

where $n_i(\chi)$ is the radial distribution of source galaxies in bin i. In the case of no anisotropic stress, the convergence power spectrum can be written in the usual form

$$P_{ij}^\kappa(\ell) = \frac{9}{4} \Omega_\mathrm{m}^2 H_0^4 \int_0^\infty \frac{g_i(\chi) g_j(\chi)}{a^2(\chi)} P(\ell/\chi, \chi) \mathrm{d}\chi. \tag{4.3}$$

The convergence can also be written in terms of the correlation functions $\xi^\pm$ via

$$\xi_{i,j}^\pm(\theta) = \frac{1}{2\pi} \int \mathrm{d}\ell\, \ell\, P_{ij}^\kappa(\ell) J_{0,4}(\ell\theta), \tag{4.4}$$

where $J_{0,4}$ are Bessel functions of the zeroth and fourth order respectively.

In figure 2 we plot the predictions for $C_\ell^{\phi\phi}$ spectrum and galaxy correlation function ξ^+, for the TDI $\mathcal{L}(g)$ and GSF models (for simplicity we take α, β_1 to be constants and $\beta_2 = 1 - \beta_1$, which removes the $\ddot{h}$-term). For galaxy lensing, we use a single redshift bin with $\xi^\pm \equiv \xi_{1,1}^\pm$ distribution of source galaxies from the Canada-France-Hawaii Telescope Lensing Survey (CFHTLenS) [12]. For illustration we have applied corrections from the Halofit fitting formulae [51, 52] to the lensing potential P_Ψ. However, since we do not have a full understanding of dark energy perturbations on non-linear scales, we do not include those scales where this correction is significant to obtain constraints on the equations of state in the next section. We compare these predictions to CMB lensing data from *Planck* [7] and the South Pole Telescope (SPT) [6], and also plot the single-bin observations from CFHTLenS.

It is clear that there will be ranges of parameter space which yield observational spectra which are compatible with the present data and therefore will not be distinguishable at present. It is most interesting to note that some of the spectra for CMB lensing are compatible with the data, but are incompatible with the galaxy weak lensing observations: the CFHTLenS galaxy weak lensing data alone could rule out a range of parameter space.

In figure 3 we plot the fractional differences in observational spectra for GSF models with a range of values of α, β_1 and β_2, relative to a fiducial quintessence scenario with $\alpha = 1$, $\beta_1 = 1$ and $\beta_2 = 0$. For all of the models shown, the differences in the C_ℓ^{TT} spectra

(a) TDI $\mathcal{L}(g)$ models

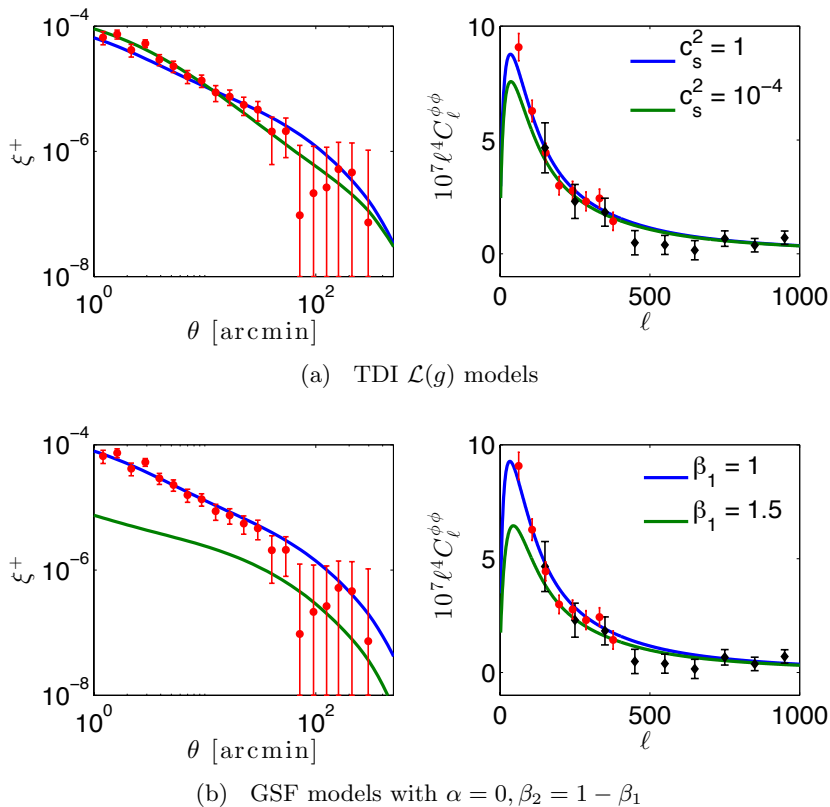(b) GSF models with $\alpha = 0, \beta_2 = 1 - \beta_1$

figure 2. Sample lensing spectra in the TDI $\mathcal{L}(g)$ and GSF models with $w = -0.8$. On the left we plot the predictions of the weak lensing correlation ξ^+ spectra, as well as the data taken from CFHTLenS. On the right we plot the lensing spectra of the CMB, $C_\ell^{\phi\phi}$, with observational data from *Planck* (red/circles) and SPT (black/diamonds). Here we see that decreasing the sound speed decreases the large-scale clustering of the dark energy.

are negligible for angular scales $\ell > 50$, that is, in the noise dominated regime. However, the differences for the CMB lensing $C_\ell^{\phi\phi}$ spectra remain roughly constant for all scales and, markedly, differences in the ξ^+ spectra increase with angular size. It is clear that models with an increased power in the spectrum of galaxy weak lensing, ξ^+, also have an increased power in the spectrum of CMB lensing, $C_\ell^{\phi\phi}$. This plot nicely illustrates how useful lensing data is, compared to the CMB temperature data where the differences between the spectra are only significant in the cosmic variance limited regime. The fundamental reason for this is that the lensing data is very sensitive to the evolution of perturbations of the dark sector theory.

It is important to have a handle on which probes are sensitive to which types of theories, and so it is useful to evaluate other probes of dark sector theories which are rather prolific in the literature. We use our modified version of CAMB to compute the sum and difference of the gravitational potentials, ϕ and ψ, the effective gravitational coupling μ, defined via

$$k^2\psi = -4\pi G\mu a^2 \left(\rho_{\mathrm{k}}\Delta_{\mathrm{k}} + 3(\rho_{\mathrm{k}} + P_{\mathrm{k}})\sigma_{\mathrm{k}}\right), \tag{4.5}$$

in which Δ is the comoving density perturbation and a subscript "k" denotes a known non-dark-sector component, and the growth function [53, 54] γ,

$$\gamma \equiv \frac{1}{\ln\Omega_{\mathrm{m}}} \ln\left(\frac{\mathrm{d}\ln\delta_{\mathrm{m}}}{\mathrm{d}\ln a}\right). \tag{4.6}$$
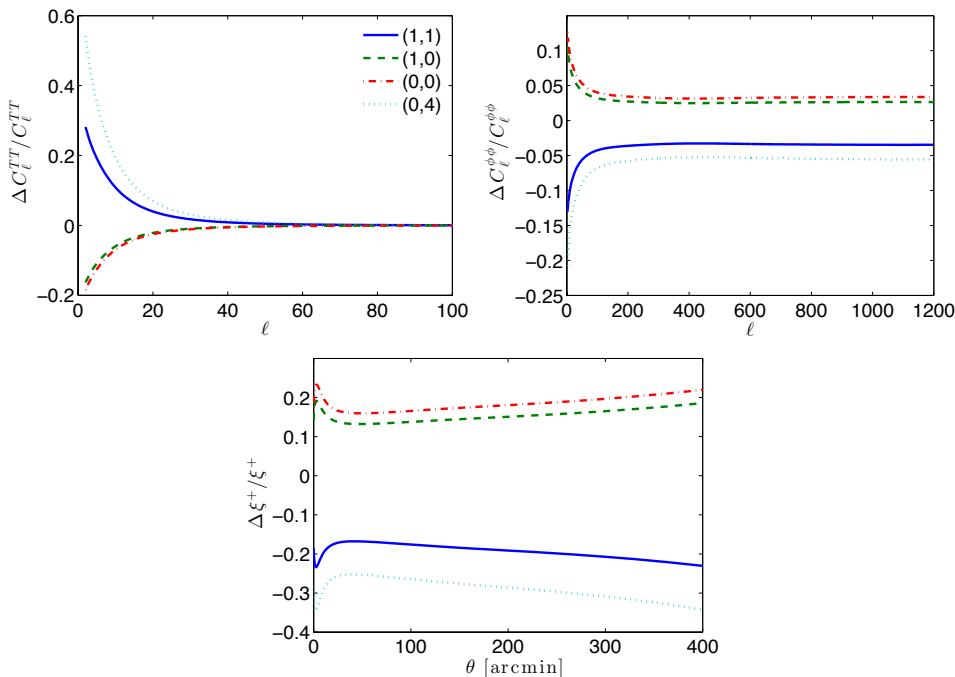
figure 3. The fractional differences in observable spectra for GSF models with various values of (β_1, β_2), relative to a quintessence scenario. $w = -0.8$ and $\alpha = 0$ are used throughout. Notice that the fractional shifts in spectra become suppressed for $\ell > 50$ in the CMB temperature spectrum C_ℓ^{TT}, remain roughly constant in the lensing of the CMB spectrum, $C_\ell^{\phi\phi}$ and grow as a function of θ for the galaxy weak lensing correlation function ξ^+.

In figure 4 we plot these quantities as a function of scale and redshift, for (a) GSF models and (b) TDI $\mathcal{L}(g)$ models. In the GSF models, the growth function γ and effective gravitational coupling μ are close to being scale independent. In contrast, both μ and γ have clear scale dependence for the TDI $\mathcal{L}(g)$ models. This serves to show that a scale-independent parameterization of the gravitational coupling μ and growth function γ would have completely missed the potential observable effects of (in this instance) TDI $\mathcal{L}(g)$ models, which is a large class of models to be insensitive to.

In figure 5 we plot the lensing potential in the TDI $\mathcal{L}(g)$ models, for various values of the sound speed, c_s^2. These plots illustrate that the lensing potential has late-time enhancements at different scales depending on the value of c_s^2. For large values of c_s^2 the lensing potential is enhanced on large scales, and for small values of c_s^2 it is enhanced on small scales. This becomes interesting when one realises that CMB lensing and galaxy weak lensing probe the lensing potential on large and small scales, respectively. Hence, data from these two types of experiments can probe different regimes. In the next section we will show our parameter constraints from using current CMB lensing and weak galaxy lensing which corroborates this point. We have performed a similar analysis when varying the α parameter in the GSF models: for $0 \leq \alpha \leq 1$ we find no qualitative difference in the lensing potential from that we presented in figure 4(a) — there certainly aren't any features which pop up on small and large scales as there are in the TDI $\mathcal{L}(g)$ models. The qualitative difference of the behavior of the lensing potential in the TDI $\mathcal{L}(g)$ and GSF models appears to be a consequence of the theoretical understanding developed in section 3.
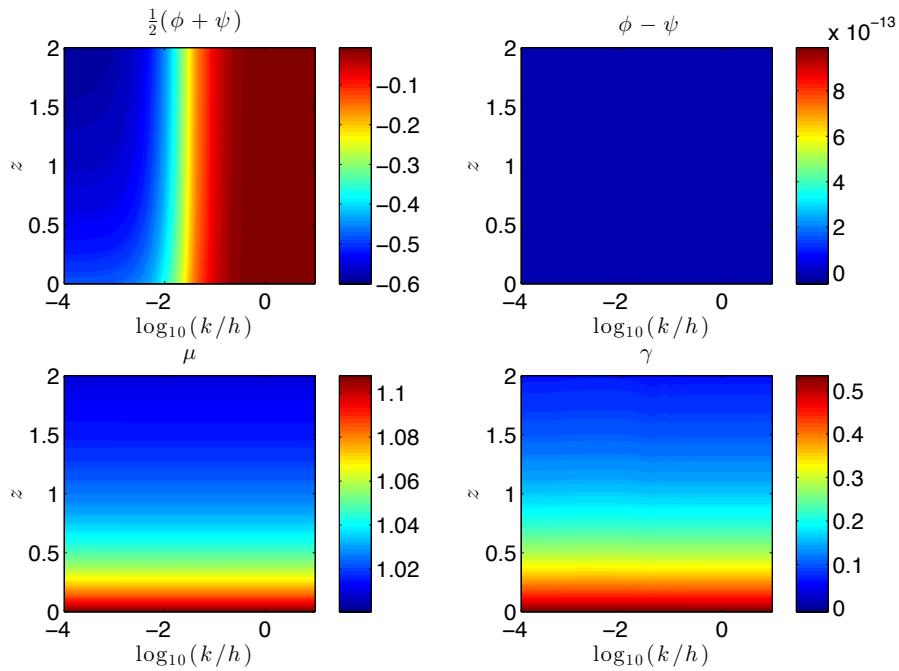
(a) GSF model with $(\alpha, \beta_1, \beta_2) = (0, 1, 0)$
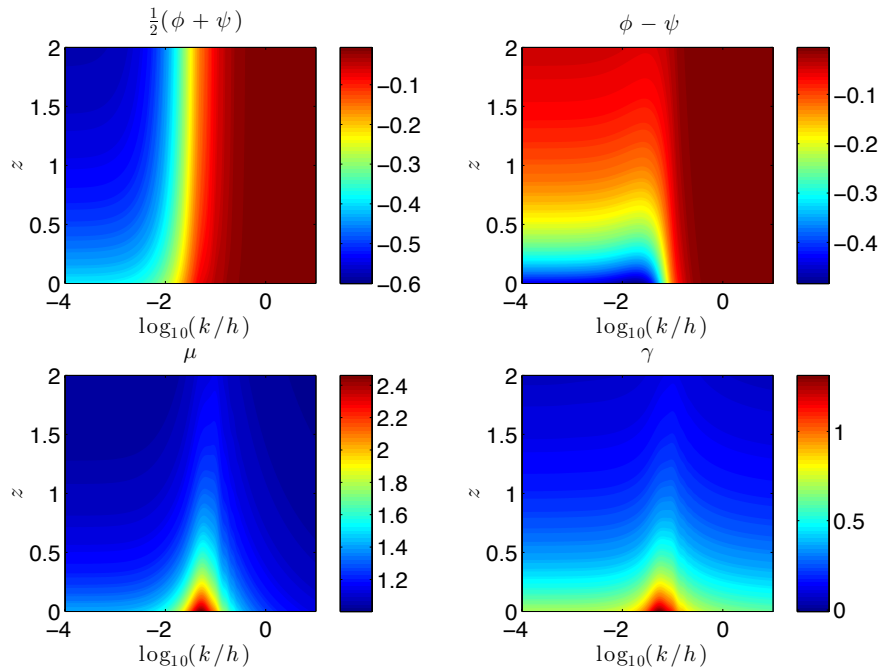
(b) TDI $\mathcal{L}(g)$ model with $c_s^2 = 10^{-3}$

figure 4. Common observational "diagnostics", as functions of scale k/h and redshift z, for two different models with $w = -0.8$. On the top row we plot the lensing potential $\psi + \phi$ and stress $\phi - \psi$, and on the bottom row we plot the effective gravitational coupling μ, and growth function γ.
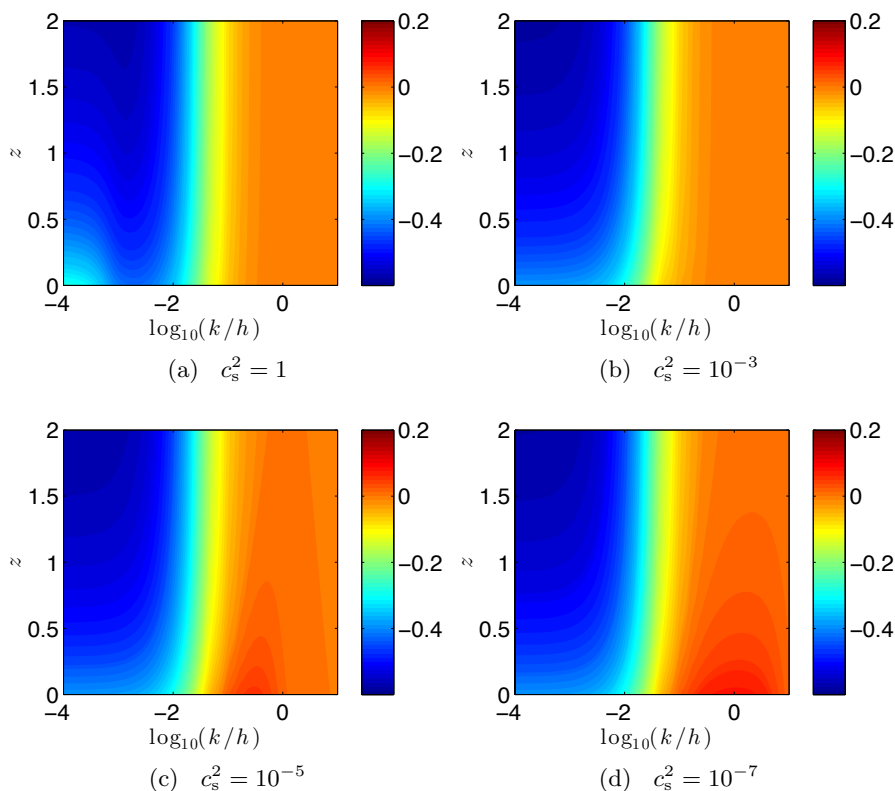
figure 5. Lensing potential $\frac{1}{2}(\phi + \psi)$ as a function of scale k/h and redshift z, in the $\mathcal{L}(g)$ TDI models for various values of the sound speed c_{s}^2 (all have $w = -0.8$). The enhacement in lensing at large scales in (a) can be picked up by observations of CMB lensing; this enhancement vanishes in (b). A new enhancement appears at small scales in (c), and has grown in (d); whilst CMB lensing is insensitive to these scales, galaxy weak lensing becomes sensitive.

5 Present data constraints

In order to place constraints on the dark sector equations of state, we use observations of temperature anisotropies in the Cosmic Microwave Background (CMB) from the *Planck* satellite [9] and polarisation measurements from the Wilkinson Microwave Anisotropy Probe (WMAP) [8]. Since the acoustic scale of the CMB is degenerate with the background equation of state w and the Hubble parameter $H_0 = 100 \, h \, \mathrm{km \, sec^{-1} \, Mpc^{-1}}$, we use observations of Baryonic Acoustic Oscillations (BAO's) from 6dF [55], SDSS (corrected for galaxy peculiar velocities) [56] and BOSS [57] to constrain the expansion history and exclude models with w far from -1 as done in the Planck analysis [5].

The dark sector perturbations are constrained by the large angle Integrated Sach Wolfe (ISW) component of the primary CMB, and gravitational lensing along the line of sight. We use CMB lensing as detected by *Planck* [7], SPT [6], and also from weak galaxy lensing detected by CFHTLenS [11, 12] to constrain the latter.

The base cosmology we consider is a 7 parameter $\mathbf{p} = \{\Omega_{\mathrm{b}}h^2, \Omega_{\mathrm{c}}h^2, \theta_{\mathrm{MC}}, A_{\mathrm{S}}, n_{\mathrm{S}}, \tau, w\}$ model. Here Ω_{b} and Ω_{c} are the baryonic and cold dark matter densities relative to the critical density, θ_{MC} is the acoustic scale of the CMB, A_{S} and n_{S} are the amplitude and spectral index of initial fluctuations respectively, and τ the optical depth to reionization. We consider

Parameter	Prior range
w	[-1.5, -0.5]
$\log_{10} c_{\mathrm{s}}^2$	[-4, 0]
$\log_{10} \alpha$	[-5, 0]
β_1	[0, 1.9]
β_2	[0, 15]

Table 1. Prior ranges on the dark energy equations of state.

both the TDI $\mathcal{L}(g)$ model, which is has one additional parameter c_{s}^2, and the GSF model with additional parameters $\{\alpha, \beta_1, \beta_2\}$.

We make use of the *Planck* likelihood [10] and follow the same procedure as the *Planck* cosmology analysis [5], that includes a number of nuisance parameters describing the contamination from our own galaxy, extragalactic sources and the SZ effect. We consider three data combinations,

   I *Planck* CMB+WP+BAO+CMB lensing,

  II *Planck* CMB+WP+BAO+CFHTLenS, and

 III *Planck*+WP+BAO+CFHTLenS+CMB lensing.

For CFHTLenS we use the shear correlation functions and covariance matrix as described in [12]. However, we make a conservative choice of angular scales to include in the analysis. Since we do not have a full understanding of how the dark energy models considered here may cluster on non-linear scales, we do not include those scales which contribute significantly to the shear correlation in the likelihood. In practice, we exclude the entire ξ^- data, and only include ξ^+ for $\theta > 12$ arcminutes. This exclusion regime was obtained by switching non-linear corrections on and off, to find the range of θ for which the ξ^+ spectrum is unaffected. This eliminates the need to apply any non-linear corrections, such as `Halofit`. For SPT lensing data we follow the same procedure as in [6], rescaling the diagonals elements of the covariance matrix according to sample variance, and adding an additional calibration-induced uncertainty to the covariance. The non-linear correction to the CMB lensing is small enough to safely ignore it.

Parameter constraints were obtained from Markov Chain Monte Carlo (MCMC) chains produced using the `COSMOMC` code [58]. Prior ranges on parameters were chosen to sufficiently contain the relevant posterior distributions. For the dark energy equations of state, these are given in table 1. We note that, formally, the equations of state that we have used are not defined for $w < -1$, but solving the equations of motion appears to give stable solutions and hence we include them as a "continuation" of physical models. Convergence of the MCMC chains was ensured by terminating the runs when the Gelman and Rubin `R-1` value, characterising the variance between chains, was < 0.05.

2D posterior likelihoods are shown in figures 6 and 7 for the two dark energy parameterizations we have considered. Constraints on the background equation of state w are consistent with previous studies combining CMB + BAO data that use a different prescription for dealing with the perturbations [59–61]. However, one of the encouraging points of this paper is that *current* observations can also constrain the parameters of the perturbative
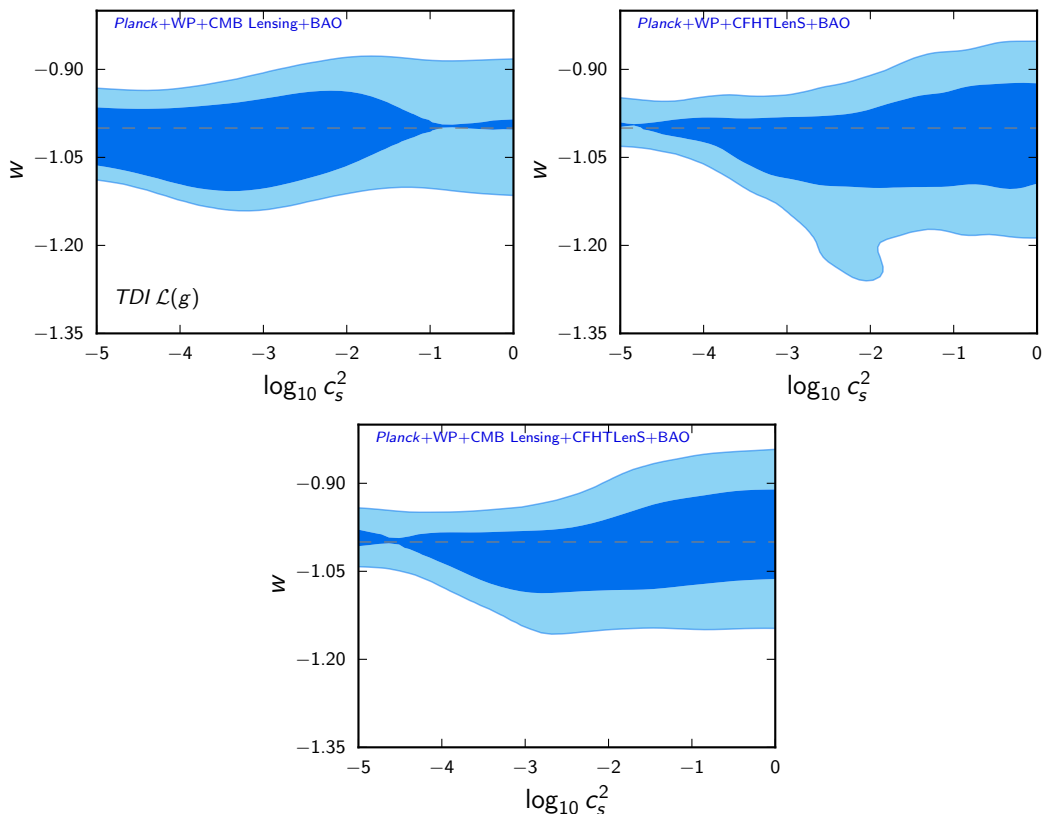
figure 6. Constraints on the (background) equation of state parameter w and the squared sound speed c_s^2 for the TDI $\mathcal{L}(g)$ model for three different data combinations. Data used in the analysis are *Planck* CMB temperature and WMAP polarization, BAO, together with either CMB lensing from *Planck* and SPT (top left panel, I), galaxy lensing from CFHTLenS (top right panel, II), and a combination of CMB lensing from *Planck* and galaxy lensing from CFHTLenS (bottom panel, III). CFHTLenS data is truncated to the linear regime, as discussed in the text.

equations of state. In the TDI $\mathcal{L}(g)$ model, shown in figure 6, a low sound speed results in clustering of the dark energy fluid on scales probed by observations. However, since in the limit of $w \to -1$ the fluid behaves like Λ, which is smooth with no perturbations, one observes a narrow valley around $w = -1$ in which c_s^2 cannot be constrained.

Similar behaviour is also observed in the generalised scalar field model, shown in figure 7. In this case α, which acts as the sound speed in quintessence models, does not result as strong clustering even when $\alpha \to 0$ as in the case of TDI $\mathcal{L}(g)$, implying that it cannot be constrained by current observations. However, varying β_1 and β_2 can lead to observable effects as shown in figure 2 and hence be constrained, as long as w is sufficiently far from $w = -1$.

There are two interesting models which are included within our GSF class of models. The first are all models whose Lagrangian is $\mathcal{L} = \mathcal{L}(\phi, \mathcal{X})$: as remarked above, these models have $\beta_1 = 1, \beta_2 = 0$, and α (which in general is a function of time) is the only free function which controls the evolution of perturbations. In figure 8 we present constraints on w and α for these models (both are assumed to be constant). It is apparent that constraints on α are almost independent of α. One should compare these constraints with the top panel of figure 7, which are for the full GSF model parameters: those show some non-trivial constraints on low values of α. The differences are non-trivial impact of the constraints on β_1 and β_2.
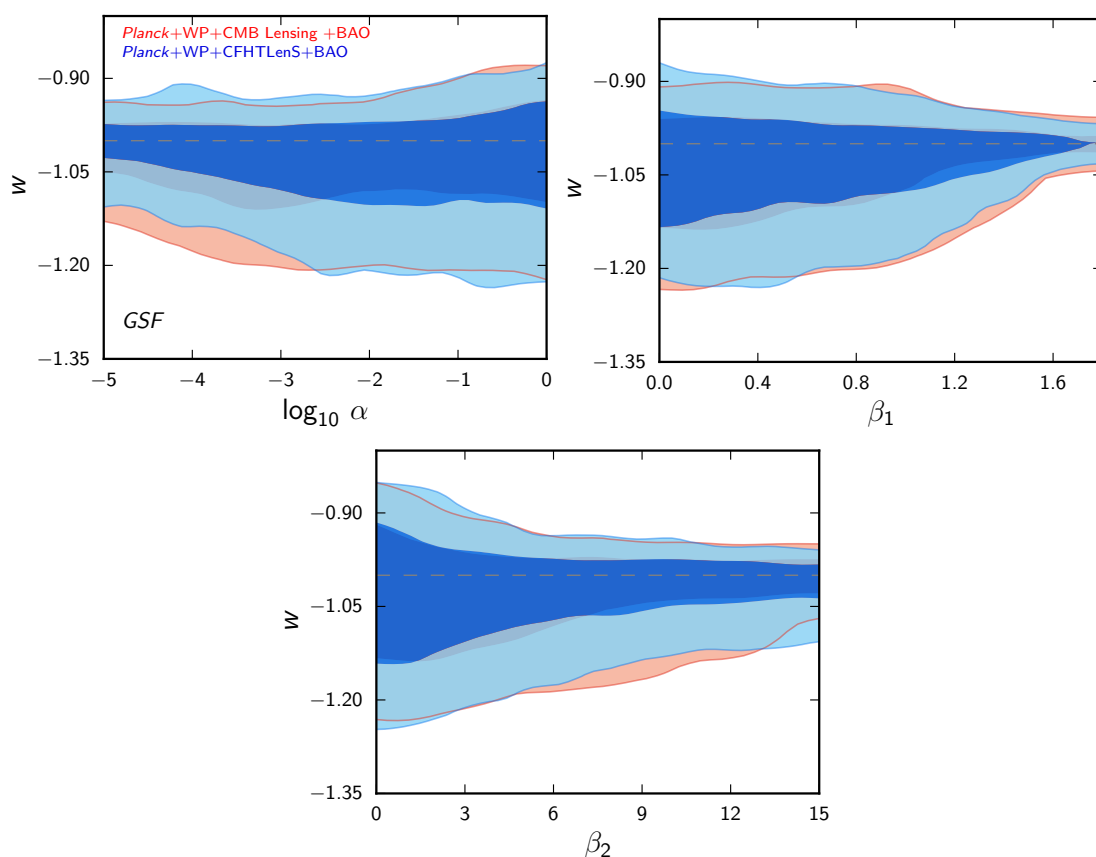
figure 7. Constraints on w and α, β_1, β_2 for the generalised scalar field model. Labelling is the same as in figure 6.
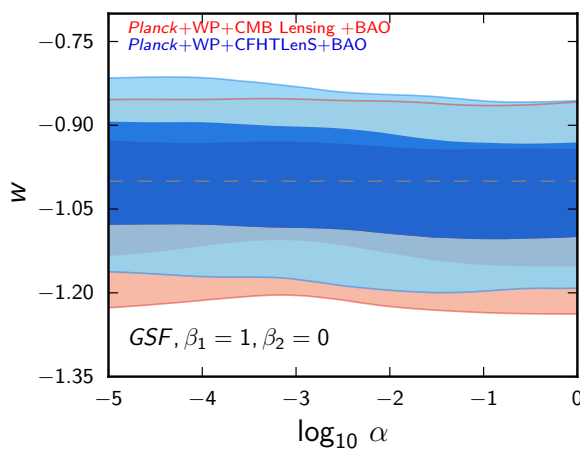

figure 8. Constraints on w and α for the generalised scalar field model with $\beta_1 = 1, \beta_2 = 0$: this correspond to models of k-essence type. Note that the constraint on w appears to be almost independent of α.
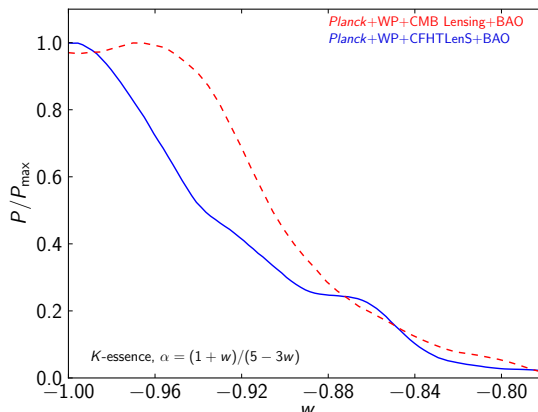
figure 9. Constraints on the equation of state parameter, w, for k-essence models with the condition that $\alpha = (1 + w)/(5 - 3w)$, that is, for the model presented in (2.11) and (2.12). Note that it is not possible for w to be < -1 in this models. This is a 1D section through the 2D likelihood presented in figure 8.

The second interesting subset of models are those with $\alpha = (1 + w)/(5 - 3w), \beta_1 = 1, \beta_2 = 0$ which were explained at the end of section 2.2.1; constraints on w are presented in figure 9.

5.1 Constraints with prejudices and priors on w

The parameters in the equations of state for perturbations become difficult to constrain when $w \approx -1$. However, it is apparent from the constraints shown in figures 6 and 7 that there are some preferred values of the parameters when $w \neq -1$. It is conceivable that an observation of background cosmology alone will constrain w. If the central value of this constraint lies away from $w = -1$ then observations of the perturbed Universe can be used to place more stringent bounds on the parameters in the equations of state for perturbations than if w is "totally free", as it has been in the previous section.

First, suppose that the data preferred some value of w; for concreteness we will pick $w = -0.95 \pm 0.01$. Then the constraints on the GSF parameters are: $\beta_1 < 1.3$ for all data combinations, and $\beta_2 < 13$ and $\beta_2 < 11$ for the $Planck$+WP+BAO+CFHTLenS and $Planck$+WP+BAO+CMB lensing data combinations respectively. In the TDI $\mathcal{L}(g)$ case only the former data combination yields a useful constraint, and we find $\log_{10} c_s^2 < -4$ is ruled out.

Secondly, by applying the prior $|1 + w| > 0.05$ we can remove the region of parameter space in which there is little clustering. In figure 10 we show the constraints on c_s^2 in the TDI $\mathcal{L}(g)$ models and in figure 11 the constraints on α, β_1, β_2 in the GSF models. After inspecting figure 11, our result for the GSF model is that the following ranges of parameter space are ruled out:

$$\beta_1 > 1.47 - 0.03(\log_{10} \alpha)^2, \tag{5.1a}$$

$$\beta_2 > 33.5 + 11.5 \log_{10} \alpha + 1.1(\log_{10} \alpha)^2, \tag{5.1b}$$

$$\beta_2 > 15(1.6 - \beta_1). \tag{5.1c}$$

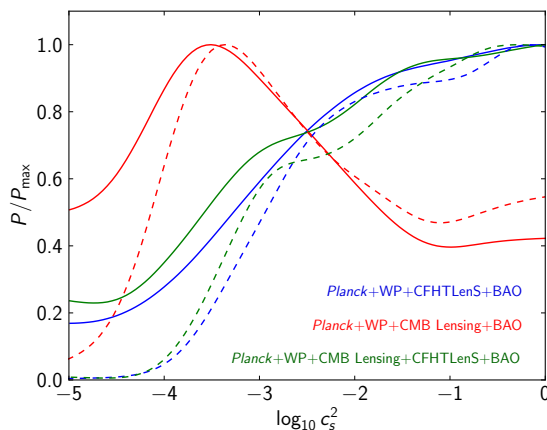In future work we will compute $\{\alpha, \beta_1, \beta_2\}$ for specific models.

figure 10. Marginalized 1D likelihoods for the sound speed parameter, $c_{\rm s}^2$, for the TDI $\mathcal{L}(g)$ model. The solid lines have no prior on w (other than that in table 1), and the dashed lines have the prior $|1 + w| > 0.05$.

6 Future constraints

The aim in this section is to determine how well upcoming experiments, such as *Euclid* [62], PRISM [20], and CoRE [21], might be able to distinguish different values of the parameters in the equations of state for perturbations. This will provide an opportunity to compare the effectiveness of CMB experiments against galaxy weak lensing experiments, and how improvements in the understanding of non-linear physics could strengthen constraints.

In order to do this, we will compare the observational spectra from two different models: one of these will be our fiducial model, which we take to be quintessence. The other model will be either a TDI $\mathcal{L}(g)$ model with a given value of $c_{\rm s}^2$, or a GSF model with a given combination of the parameter values $\{\alpha, \beta_1, \beta_2\}$. We will compute the χ^2 between the spectra of the two models. This will be done for CMB-type experiments, where the data included are the temperature, polarization, and CMB lensing spectra, and tomographic galaxy weak lensing experiments, where the data included is the convergence power spectra correlated across different redshift bins. The χ^2 will indicate the potential discriminatory power; below we explain how χ^2 is computed for the CMB and tomographic galaxy weak lensing experiments.

At each multipole ℓ-mode we compute the $n \times n$ covariance matrix $P_{ij}(\ell)$ for a given type of observation (e.g. CMB or galaxy weak lensing). The covariance matrices for two models, $\widehat{P}_{ij}(\ell)$ and $\overline{P}_{ij}(\ell)$ say, are modified to include experimental noise:

$$P_{ij}(\ell) \longrightarrow P_{ij}(\ell) + \mathcal{N}_{ij}(\ell). \tag{6.1}$$

The properties of the noise, $\mathcal{N}_{ij}(\ell)$, are experiment and survey dependent, but we assume they are known and diagonal. Computing the $\chi^2 \equiv -2 \ln \mathcal{L}$ between the two models yields

$$\chi^2 = \sum_{\ell=2}^{\ell_{\rm max}} f_{\rm sky}(2\ell+1)\Delta\ell \left[\widehat{P}_{ij}^{-1}\overline{P}^{ij} + \ln \left| \frac{|\widehat{P}|}{|\overline{P}|} \right| - n \right], \tag{6.2}$$

where $f_{\rm sky}$ is the fraction of the sky covered by a given survey, $\Delta\ell$ is the width of the multipole bin, $\widehat{P}_{ij}^{-1}\overline{P}^{ij} \equiv \sum_{i,j=1}^{n} \widehat{P}_{ij}^{-1}\overline{P}^{ij}$, $|P|$ denotes the determinant of P, and n is the dimension of the covariance matrix. For the weak galaxy lensing experiments, we consider a range of upper-limits $\ell_{\rm max}$ in (6.2) to represent our understanding (or lack-of) of the dark
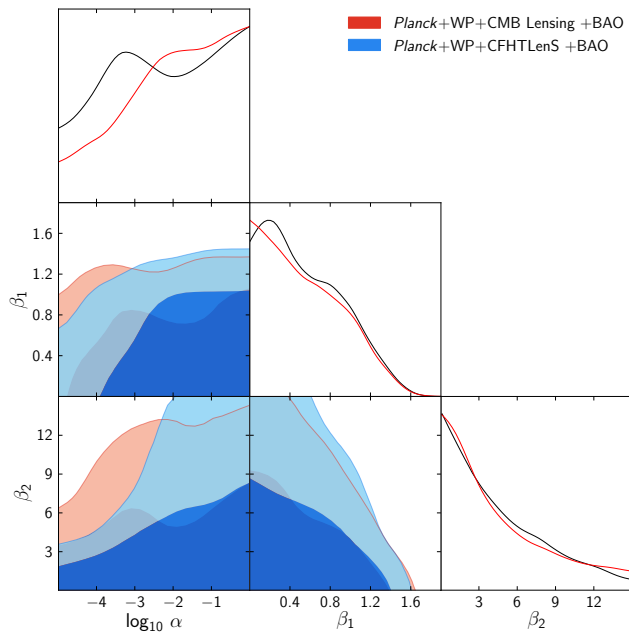
figure 11. Constraints on α, β_1, β_2 for the GSF model, using a prior of $|1 + w| > 0.05$. Constraints are qualitatively similar without using this prior.

sector on non-linear scales. These are $\ell_{\max} = 10^2$, for which non-linear effects are negligible, and $\ell_{\max} = 10^3$, for which non-linear effects come into play, but we might hope that there exists some understanding (in practice, we use `Halofit`).

For CMB experiments, the covariance matrix is constructed from the temperature T, curl-free polarization E, and deflection d correlation functions C_ℓ^{XY} according to

$$P_{ij}^{\mathrm{CMB}}(\ell) = \begin{pmatrix} C_\ell^{TT} & C_\ell^{TE} & C_\ell^{Td} \\ C_\ell^{TE} & C_\ell^{EE} & 0 \\ C_\ell^{Td} & 0 & C_\ell^{dd} \end{pmatrix}. \tag{6.3}$$

This construction is identical to that given in [63]. For galaxy weak lensing observations, the covariance matrix is computed via (4.3), and describes the correlations of the convergence spectra between N redshift bins.

For the CMB, we assume noise excepted for CoRE [21], PRISM [20], *Planck* [64] and a hypothetical cosmic variance limited experiment. For tomographic galaxy weak lensing, we use the *Euclid* RedBook[1] noise values [65], which are given in table. 2. Here the noise term is

$$\mathcal{N}_{ij} = \delta_{ij} \left\langle \gamma_{\mathrm{int}}^2 \right\rangle n_j^{-1}, \tag{6.4}$$

where γ_{int} is the rms intrinsic shear, n_i is the number of galaxies per steradians in the ith-bin, given by

$$n_i = 3600 \, d \, (180/\pi)^2 \hat{n}_i \,, \tag{6.5}$$

where d is the number of galaxies per square arcminute, and $\hat{n}_i$ is the fraction of sources in the ith-bin. We assume a radial distribution of sources to a maximum redshift $z_{\max}$, given by

$$d(z) = z^2 \exp\left[-(z/z_0)^{1.5}\right] \,, \tag{6.6}$$

_____

[1] Also see the *Euclid* website, http://www.euclid-ec.org.

Parameter	Value
$\langle \gamma_{\text{int}} \rangle^{1/2}$	0.22
d	33
N	10
$z_{\max}$	2.5
z_0	1.0

Table 2. *Euclid* survey parameters.

constructed in such a way that there are an equal number of galaxies for each of the N redshift bins. For *Euclid*, this means a constant $1.17 \times 10^{-10} N$ is added to the diagonal elements of the covariance matrix.

In figure 12 we plot the χ^2 values for the $\mathcal{L}(g)$ TDI models for CMB and tomographic weak lensing experiments. It is perhaps interesting to note that the tomographic weak lensing surveys alone will allow us to probe very low values of the sound speed parameter. The level of the constraining power clearly increases as $\ell_{\max}$ is increased.

In figure 13 we plot the χ^2 values for various GSF models — in the plots we fixed the value $\alpha = 10^{-5}$, and varied β_1 and β_2. We can see that the constraining power of PRISM compared to the "ultimate limit" of cosmic variance limited CMB experiments are very similar. There will always be a degeneracy in measuring β_1 for low values of β_2. In the tomographic weak lensing case, increasing $\ell_{\max}$ from 10^2 to 10^3 breaks this degeneracy in β_1 for low values of β_2.

7 Conclusions

In this paper we presented constraints from current data on the equations of state for perturbations in two distinct classes of models: the GSF and TDI $\mathcal{L}(g)$ models. In addition we have explored how well future experiments will be able to constrain the parameters and how further understanding non-linearities will help break observational degeneracies. We presented analytic arguments explaining how the lensing potential should be expected to look rather different in models with and without anisotropic stress.

Our constraints using the *Planck*+WP+ BAO+CFHTLenS data in the TDI $\mathcal{L}(g)$ model appears to suggest that $c_s^2 > 10^{-4}$ which implies that the Jeans length of the effective dark sector fluid is $> 30 h^{-1}$ Mpc. This can also constitute a constraint on the masses of gravitons in the corresponding Lorentz violating massive gravity scenario [37]. There the graviton masses m_i^2 are given in terms of w, c_s^2

$$m_0^2 = -M^2, \tag{7.1a}$$

$$m_1^2 = -\frac{1}{4} w M^2, \tag{7.1b}$$

$$m_2^2 = -\frac{1}{2} \left[w + \frac{3}{4}(1+w)(c_s^2 - w) \right] M^2, \tag{7.1c}$$

$$m_3^2 = \frac{1}{4} \left[w^2 - \frac{1}{2} \left(c_s^2 - w \right) (1+w) \right] M^2, \tag{7.1d}$$

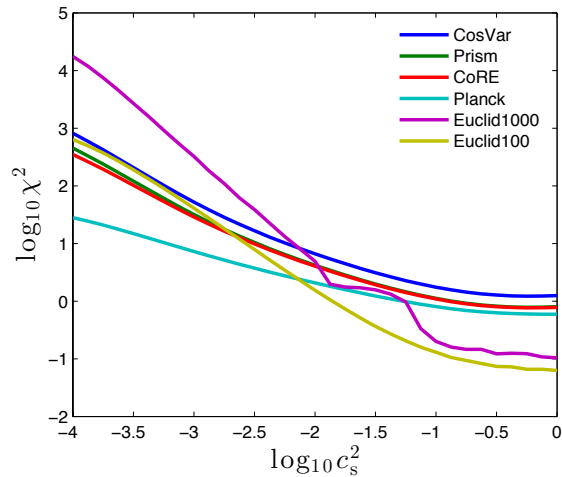$$m_4^2 = -\frac{1}{2} w M^2, \tag{7.1e}$$

figure 12. Comparing the discriminatory power of CMB and galaxy weak lensing experiments for the sound speed parameter c_s^2 in the TDI $\mathcal{L}(g)$ models. We plot χ^2 for CMB experiments with cosmic variance, PRISM, CoRE, and *Planck* noises, and tomographic galaxy weak lensing measurements using *Euclid* survey parameters with $\ell_{max} = 10^2, 10^3$ respectively. We have used a fiducial cosmological model with $w = -0.8$.
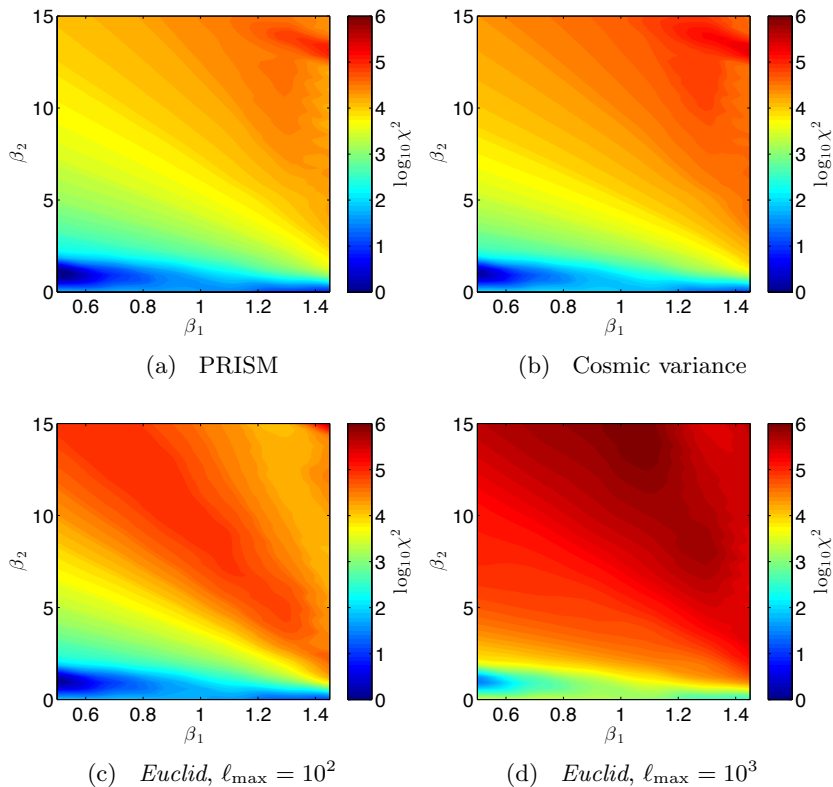

(a) PRISM

(b) Cosmic variance

(c) *Euclid*, $\ell_{max} = 10^2$

(d) *Euclid*, $\ell_{max} = 10^3$

figure 13. Potential discriminatory power of the GSF models; here we have fixed $\alpha = 10^{-5}$ and varied β_1 and β_2 as shown in the axes. In (a) and (b) we use CMB experiments — with PRISM and cosmic variance limited noises, and in (c) and (d) we use tomographic weak lensing experiments — with *Euclid* noises and with a maximum multipole $\ell_{max} = 10^2$ and $\ell_{max} = 10^3$ respectively.

and a mass scale M^2 defined by $\Omega_{\rm de} = M^2/(3H_0^2)$. Hence, the constraints on w and $c_{\rm s}^2$ we gave in figure 6 can be used to constrain the m_i^2.

The results outlined in this paper are encouraging since we are able to constrain parameterizations of dark energy and modified gravity using current linear data. In some sense this success is due to our parameterization being phrased at the level of effective fluid equations which directly govern the evolution of observable quantities, rather than at the level of the action or gravitational field equations — although there is a correspondance between these approaches.

Acknowledgments

References

[1] E.J. Copeland, M. Sami and S. Tsujikawa, *Dynamics of dark energy*, *Int. J. Mod. Phys.* **D 15** (2006) 1753 [hep-th/0603057] [INSPIRE].

[2] T. Clifton, P.G. Ferreira, A. Padilla and C. Skordis, *Modified Gravity and Cosmology*, *Phys. Rept.* **513** (2012) 1 [arXiv:1106.2476] [INSPIRE].

[3] SUPERNOVA COSMOLOGY PROJECT collaboration, S. Perlmutter et al., *Measurements of Omega and Lambda from 42 high redshift supernovae*, *Astrophys. J.* **517** (1999) 565 [astro-ph/9812133] [INSPIRE].

[4] SUPERNOVA SEARCH TEAM collaboration, A.G. Riess et al., *Observational evidence from supernovae for an accelerating universe and a cosmological constant*, *Astron. J.* **116** (1998) 1009 [astro-ph/9805201] [INSPIRE].

[5] PLANCK collaboration, P.A.R. Ade et al., *Planck 2013 results. XVI. Cosmological parameters*, *Astron. Astrophys.* **571** (2014) A16 [arXiv:1303.5076] [INSPIRE].

[6] A. van Engelen, R. Keisler, O. Zahn, K.A. Aird, B.A. Benson et al., *A measurement of gravitational lensing of the microwave background using South Pole Telescope data*, *Astrophys. J.* **756** (2012) 142 [arXiv:1202.0546] [INSPIRE].

[7] PLANCK collaboration, P.A.R. Ade et al., *Planck 2013 results. XVII. Gravitational lensing by large-scale structure*, *Astron. Astrophys.* **571** (2014) A17 [arXiv:1303.5077] [INSPIRE].

[8] WMAP collaboration, C.L. Bennett et al., *Nine-Year Wilkinson Microwave Anisotropy Probe (WMAP) Observations: Final Maps and Results*, *Astrophys. J. Suppl.* **208** (2013) 20 [arXiv:1212.5225] [INSPIRE].

[9] PLANCK collaboration, P.A.R. Ade et al., *Planck 2013 results. I. Overview of products and scientific results*, *Astron. Astrophys.* **571** (2014) A1 [arXiv:1303.5062] [INSPIRE].

[10] PLANCK collaboration, P.A.R. Ade et al., *Planck 2013 results. XV. CMB power spectra and likelihood*, *Astron. Astrophys.* **571** (2014) A15 [arXiv:1303.5075] [INSPIRE].

[11] C. Heymans, L. Van Waerbeke, L. Miller, T. Erben, H. Hildebrandt et al., *CFHTLenS: The Canada-France-Hawaii Telescope Lensing Survey*, *Mon. Not. Roy. Astron. Soc.* **427** (2012) 146 [arXiv:1210.0032] [INSPIRE].

[12] M. Kilbinger, L. Fu, C. Heymans, F. Simpson, J. Benjamin et al., *CFHTLenS: Combined probe cosmological model comparison using 2D weak gravitational lensing*, *Monthly Notices of the Royal Astronomical Society* **430** (2013) 2200 [arXiv:1212.3338] [INSPIRE].

[13] R. Bean and O. Dore, *Probing dark energy perturbations: The Dark energy equation of state and speed of sound as measured by WMAP*, *Phys. Rev.* **D 69** (2004) 083503 [astro-ph/0307100] [ɪɴSPIRE].

[14] G. Ballesteros and J. Lesgourgues, *Dark energy with non-adiabatic sound speed: initial conditions and detectability*, *JCAP* **10** (2010) 014 [arXiv:1004.5509] [ɪɴSPIRE].

[15] R. de Putter, D. Huterer and E.V. Linder, *Measuring the Speed of Dark: Detecting Dark Energy Perturbations*, *Phys. Rev.* **D 81** (2010) 103513 [arXiv:1002.1311] [ɪɴSPIRE].

[16] V. Salvatelli, A. Marchini, L. Lopez-Honorez and O. Mena, *New constraints on Coupled Dark Energy from the Planck satellite experiment*, *Phys. Rev.* **D 88** (2013) 023531 [arXiv:1304.7119] [ɪɴSPIRE].

[17] J.-Q. Xia, H. Li and X. Zhang, *Dark Energy Constraints after Planck*, *Phys. Rev.* **D 88** (2013) 063501 [arXiv:1308.0188] [ɪɴSPIRE].

[18] A. Marchini and V. Salvatelli, *Updated constraints from the PLANCK experiment on modified gravity*, *Phys. Rev.* **D 88** (2013) 027502 [arXiv:1307.2002] [ɪɴSPIRE].

[19] B. Hu, M. Liguori, N. Bartolo and S. Matarrese, *Parametrized modified gravity constraints after Planck*, *Phys. Rev.* **D 88** (2013) 123514 [arXiv:1307.5276] [ɪɴSPIRE].

[20] PRISM collaboration, P. Andre et al., *PRISM (Polarized Radiation Imaging and Spectroscopy Mission): A White Paper on the Ultimate Polarimetric Spectro-Imaging of the Microwave and Far-Infrared Sky*, arXiv:1306.2259 [ɪɴSPIRE].

[21] COʀE collaboration, F.R. Bouchet et al., *COrE (Cosmic Origins Explorer) A White Paper*, arXiv:1102.2181 [ɪɴSPIRE].

[22] Dark Energy Survey collaboration, T. Abbott et al., *The dark energy survey*, astro-ph/0510346 [ɪɴSPIRE].

[23] EUCLID collaboration, R. Laureijs et al., *Euclid Definition Study Report*, arXiv:1110.3193 [ɪɴSPIRE].

[24] LSST Dark Energy Science collaboration, A. Abate et al., *Large Synoptic Survey Telescope: Dark Energy Science Collaboration*, arXiv:1211.0310 [ɪɴSPIRE].

[25] R. Bean and M. Tangmatitham, *Current constraints on the cosmic growth history*, *Phys. Rev.* **D 81** (2010) 083534 [arXiv:1002.4197] [ɪɴSPIRE].

[26] L. Pogosian, A. Silvestri, K. Koyama and G.-B. Zhao, *How to optimally parametrize deviations from General Relativity in the evolution of cosmological perturbations?*, *Phys. Rev.* **D 81** (2010) 104023 [arXiv:1002.2382] [ɪɴSPIRE].

[27] T. Baker, P.G. Ferreira, C. Skordis and J. Zuntz, *Towards a fully consistent parameterization of modified gravity*, *Phys. Rev.* **D 84** (2011) 124018 [arXiv:1107.0491] [ɪɴSPIRE].

[28] J. Zuntz, T. Baker, P. Ferreira and C. Skordis, *Ambiguous Tests of General Relativity on Cosmological Scales*, *JCAP* **06** (2012) 032 [arXiv:1110.3830] [ɪɴSPIRE].

[29] T. Baker, P.G. Ferreira and C. Skordis, *The Parameterized Post-Friedmann framework for theories of modified gravity: concepts, formalism and examples*, *Phys. Rev.* **D 87** (2013) 024015 [arXiv:1209.2117] [ɪɴSPIRE].

[30] E.-M. Mueller, R. Bean and S. Watson, *Cosmological implications of the effective field theory of cosmic acceleration*, *Phys. Rev.* **D 87** (2013) 083504 [arXiv:1209.2706] [ɪɴSPIRE].

[31] M. Kunz, *The phenomenological approach to modeling the dark energy*, *Comptes Rendus Physique* **13** (2012) 539 [arXiv:1204.5482] [ɪɴSPIRE].

[32] A. Silvestri, L. Pogosian and R.V. Buniy, *Practical approach to cosmological perturbations in modified gravity*, *Phys. Rev.* **D 87** (2013) 104015 [arXiv:1302.1193] [ɪɴSPIRE].

[33] M. Motta, I. Sawicki, I.D. Saltas, L. Amendola and M. Kunz, *Probing Dark Energy through Scale Dependence*, *Phys. Rev.* **D 88** (2013) 124035 [arXiv:1305.0008] [inSPIRE].

[34] B. Soergel, T. Giannantonio, J. Weller and R.A. Battye, *Constraining dark sector perturbations II. ISW and CMB lensing tomography*, in preparation (2014).

[35] R.A. Battye and J.A. Pearson, *Effective action approach to cosmological perturbations in dark energy and modified gravity*, *JCAP* **07** (2012) 019 [arXiv:1203.0398] [inSPIRE].

[36] J.A. Pearson, *Effective field theory for perturbations in dark energy and modified gravity*, arXiv:1205.3611 [inSPIRE].

[37] R.A. Battye and J.A. Pearson, *Massive gravity, the elasticity of space-time and perturbations in the dark sector*, *Phys. Rev.* **D 88** (2013) 084004 [arXiv:1301.5042] [inSPIRE].

[38] R.A. Battye and J.A. Pearson, *Parametrizing dark sector perturbations via equations of state*, *Phys. Rev.* **D 88** (2013) 061301 [arXiv:1306.1175] [inSPIRE].

[39] J. Bloomfield and J. Pearson, *Simple implementation of general dark energy models*, *JCAP* **03** (2014) 017 [arXiv:1310.6033] [inSPIRE].

[40] R.A. Battye and J.A. Pearson, *Computing model independent perturbations in dark energy and modified gravity*, *JCAP* **03** (2014) 051 [arXiv:1311.6737] [inSPIRE].

[41] C.-P. Ma and E. Bertschinger, *Cosmological perturbation theory in the synchronous versus conformal Newtonian gauge*, *Astrophys. J.* (1994) [astro-ph/9401007] [inSPIRE].

[42] C. Deffayet, O. Pujolàs, I. Sawicki and A. Vikman, *Imperfect Dark Energy from Kinetic Gravity Braiding*, *JCAP* **10** (2010) 026 [arXiv:1008.0048] [inSPIRE].

[43] O. Pujolàs, I. Sawicki and A. Vikman, *The Imperfect Fluid behind Kinetic Gravity Braiding*, *JHEP* **11** (2011) 156 [arXiv:1103.5360] [inSPIRE].

[44] A. Barreira, B. Li, W.A. Hellwing, C.M. Baugh and S. Pascoli, *Nonlinear structure formation in the Cubic Galileon gravity model*, *JCAP* **10** (2013) 027 [arXiv:1306.3219] [inSPIRE].

[45] J. Weller and A.M. Lewis, *Large scale cosmic microwave background anisotropies and dark energy*, *Mon. Not. Roy. Astron. Soc.* **346** (2003) 987 [astro-ph/0307104] [inSPIRE].

[46] M. Bucher and D.N. Spergel, *Is the dark matter a solid?*, *Phys. Rev.* **D 60** (1999) 043505 [astro-ph/9812022] [inSPIRE].

[47] R.A. Battye and A. Moss, *Cosmological Perturbations in Elastic Dark Energy Models*, *Phys. Rev.* **D 76** (2007) 023005 [astro-ph/0703744] [inSPIRE].

[48] M. Sitwell and K. Sigurdson, *Quantization of Perturbations in an Inflating Elastic Solid*, *Phys. Rev.* **D 89** (2014) 123509 [arXiv:1306.5762] [inSPIRE].

[49] A. Lewis, A. Challinor and A. Lasenby, *Efficient computation of CMB anisotropies in closed FRW models*, *Astrophys. J.* **538** (2000) 473 [astro-ph/9911177] [inSPIRE].

[50] A. Hojjati, L. Pogosian and G.-B. Zhao, *Testing gravity with CAMB and CosmoMC*, *JCAP* **08** (2011) 005 [arXiv:1106.4543] [inSPIRE].

[51] VIRGO Consortium collaboration, R.E. Smith et al., *Stable clustering, the halo model and nonlinear cosmological power spectra*, *Mon. Not. Roy. Astron. Soc.* **341** (2003) 1311 [astro-ph/0207664] [inSPIRE].

[52] R. Takahashi, M. Sato, T. Nishimichi, A. Taruya and M. Oguri, *Revising the Halofit Model for the Nonlinear Matter Power Spectrum*, *Astrophys. J.* **761** (2012) 152 [arXiv:1208.2701] [inSPIRE].

[53] L.-M. Wang and P.J. Steinhardt, *Cluster abundance constraints on quintessence models*, *Astrophys. J.* **508** (1998) 483 [astro-ph/9804015] [inSPIRE].

[54] E.V. Linder, *Cosmic growth history and expansion history*, *Phys. Rev.* **D 72** (2005) 043529 [astro-ph/0507263] [INSPIRE].

[55] F. Beutler, C. Blake, M. Colless, D.H. Jones, L. Staveley-Smith et al., *The 6dF Galaxy Survey: Baryon Acoustic Oscillations and the Local Hubble Constant*, *Mon. Not. Roy. Astron. Soc.* **416** (2011) 3017 [arXiv:1106.3366] [INSPIRE].

[56] N. Padmanabhan, X. Xu, D.J. Eisenstein, R. Scalzo, A.J. Cuesta, K.T. Mehta and E. Kazin, *A 2 per cent distance to z = 0.35 by reconstructing baryon acoustic oscillations — I. Methods and application to the Sloan Digital Sky Survey*, *Mon. Not. Roy. Astron. Soc.* **427** (2012) 2132 [arXiv:1202.0090] [INSPIRE].

[57] L. Anderson, E. Aubourg, S. Bailey, F. Beutler, A.S. Bolton et al., *The clustering of galaxies in the SDSS-III Baryon Oscillation Spectroscopic Survey: Measuring D_A and H at $z = 0.57$ from the Baryon Acoustic Peak in the Data Release 9 Spectroscopic Galaxy Sample*, arXiv:1303.4666 [INSPIRE].

[58] A. Lewis and S. Bridle, *Cosmological parameters from CMB and other data: A Monte Carlo approach*, *Phys. Rev.* **D 66** (2002) 103511 [astro-ph/0205436] [INSPIRE].

[59] W. Hu and I. Sawicki, *A Parameterized Post-Friedmann Framework for Modified Gravity*, *Phys. Rev.* **D 76** (2007) 104043 [arXiv:0708.1190] [INSPIRE].

[60] W. Hu, *Parametrized Post-Friedmann Signatures of Acceleration in the CMB*, *Phys. Rev.* **D 77** (2008) 103524 [arXiv:0801.2433] [INSPIRE].

[61] W. Fang, W. Hu and A. Lewis, *Crossing the Phantom Divide with Parameterized Post-Friedmann Dark Energy*, *Phys. Rev.* **D 78** (2008) 087303 [arXiv:0808.3125] [INSPIRE].

[62] EUCLID THEORY WORKING GROUP collaboration, L. Amendola et al., *Cosmology and fundamental physics with the Euclid satellite*, *Living Rev. Rel.* **16** (2013) 6 [arXiv:1206.1225] [INSPIRE].

[63] L. Perotto, J. Lesgourgues, S. Hannestad, H. Tu and Y.Y.Y. Wong, *Probing cosmological parameters with the CMB: Forecasts from full Monte Carlo simulations*, *JCAP* **10** (2006) 013 [astro-ph/0606227] [INSPIRE].

[64] PLANCK collaboration, *Planck blue book*, ESA (2005).

[65] L. Amendola, M. Kunz and D. Sapone, *Measuring the dark side (with weak lensing)*, *JCAP* **04** (2008) 013 [arXiv:0704.2421] [INSPIRE].